C-H Chalcogenation by a Bromide Rich and Environmentally Benign Orthorhombic $CsPbBr_3$ under Visible Light, Polar Media and Aerobic Condition

Ashis Mathuri[†], Buddhadeb Pal[†], Milan Pramanik, Anupam Manna* and Prasenjit Mal*

School of Chemical Sciences, National Institute of Science Education and Research (NISER) Bhubaneswar, An OCC of Homi Bhabha National Institute, PO Bhimpur-Padanpur, Via Jatni, District Khurda, Odisha 752050, India.

*Corresponding author (s): Prasenjit Mal, E-mail: pmal@niser.ac.in; and Anupam Manna, Email: anupammanna@niser.ac.in

[†]Equal contributing authors.

TOC

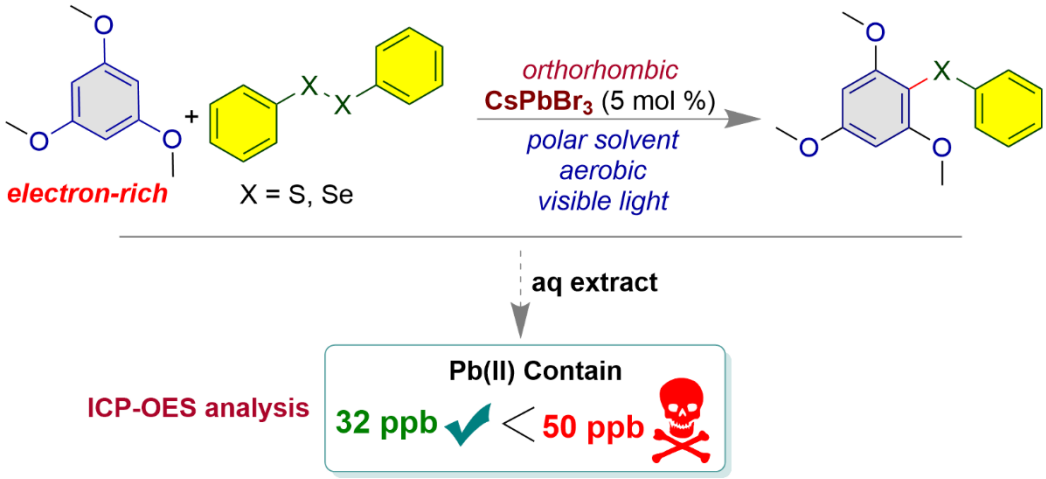

KEYWORDS

C-H Chalcogenation; Environmentally benign photocatalysis; Lead leaching; Orthorhombic $CsPbBr_3$; Colloidal perovskite stability

ABSTRACT

The stability of $CsPbBr_3$ nanocrystals (NCs) in open air remains challenging and can vary depending on the specific material and conditions. Generally, perovskites are prone to degradation due to oxygen, moisture, polar solvent, and light exposure. In this work, we have aimed to develop strategies to improve the stability of $CsPbBr_3$ perovskite and broaden its potential applications in organic synthesis. An orthorhombic $CsPbBr_3$ perovskite nano-crystal (NC) obtained from bromide precursor dibromoisocyanuric acid, can work efficiently as a visible light photocatalyst (blue LED, 5 mol % and TON ~ 18.11) under O_2 atmosphere and in acetonitrile (dielectric constant $\varepsilon \sim 37.5$). The synthesis of diaryl sulfides and a diaryl selenide were achieved *via* template-free C-H functionalization of electron-rich arenes. The electron-rich arenes also helped to enhance the stability of the $CsPbBr_3$ perovskites photocatalyst within the reaction system. The orthorhombic and bromide-rich $CsPbBr_3$ NC displayed superior photocatalytic activity than cubic $CsPbBr_3$ NCs and was found to be environmentally benign. After the reaction, only 32 ppb of Pb(II) was leached out (ICP-OES analysis) which is quite lower than the maximum permissible limit for drinking water of humans (50 ppb).

INTRODUCTION

The lead halide perovskite $CsPbBr_3$ nanocrystals (NCs) are the materials that have gained significant attention recently due to their exceptional optoelectronic properties.[1] They have shown promising potential for various applications which include solar cells,[2-5] light-emitting diodes,[6-7] lasers,[8-9] and photodetectors.[10] In addition, the perovskites are widely used as photocatalysts for H_2 generation, CO_2 reduction, N_2 fixation, dye degradation, etc.[11-14] This is due to its high absorption coefficient, tunable bandgap, and high photoluminescence quantum yield. In addition, $CsPbBr_3$ perovskite has a relatively low cost and is simple to synthesize, making it a promising material for large-scale applications.[15]

In recent times, the $CsPbBr_3$ perovskite NCs also have been explored as photocatalysts in organic synthesis.[16-21] Photocatalysis has gained interest as a green and sustainable alternative to traditional chemical synthesis methods, which often rely on high temperatures and/or harsh chemicals.[22-23] However, there are still some challenges associated with $CsPbBr_3$ perovskite, such as its long-term stability[24] and the toxicity of lead. Nevertheless, ongoing research is aimed at addressing these issues and developing more efficient and stable perovskite-based photocatalysts. The major challenges for practical utilization of the perovskites NCs as photocatalysts in organic synthesis is the instability of perovskites towards light,[25-30] moisture,[25-26, 28-29] O_2 atmosphere,[25-28] and polar solvent.[31-32]

The C-H chalcogenation is a valuable strategy for synthesizing chalcogen-containing compounds, which have a wide range of applications, including pharmaceuticals, materials science, and catalysis.[33-35] The C-H chalcogenation process can be carried out using various methods, including transition-metal catalysis,[36] photoredox catalysis,[37] and organocatalysis.[38] In recent years, significant progress has been made in the development of more efficient methods for C-H chalcogenation.[39-40] Maiti and co-workers have reported a ligand-assisted palladium-catalyzed C-H activation approach for the synthesis of chalcogens. This method utilizes palladium catalysts, which can functionalize the C-H bond of arenes and mediate the reaction with chalcogens like diaryl disulfide and diaryl diselenide (Figure 1a).[41] Lei and co-workers have identified the C-H functionalization of electron-rich arenes using stoichiometric oxidants, such as 2,3-dichloro-5,6-dicyano-1,4-benzoquinone (DDQ).[42]

RESULTS AND DISCUSSION

To the best of our knowledge, C-H chalcogenation of arenes using visible light photocatalysis is hitherto unknown. Herein, we report the synthesis of diaryl sulfides and diaryl selenide

(Figure 1c) under visible light (blue LED) using $CsPbBr_3$ NCs as photocatalyst. Moreover, the synthesis of the $CsPbBr_3$ perovskites was achieved by using hot injection methods.[43-44] The green-fluorescent orthorhombic $CsPbBr_3$ (DBIA-$CsPbBr_3$) NC was synthesized using dibromoisocyanuric acid as the bromide-precursor (Figure 1b).[45] Orthorhombic $CsPbBr_3$ perovskite is known for its high stability and improved performance in optoelectronic devices, compared to its cubic counterpart.[46] This is due to its more ordered crystal structure and improved optical properties. The cubic $CsPbBr_3$ perovskites DBHT-$CsPbBr_3$, NBS-$CsPbBr_3$ and NBA-$CsPbBr_3$ were obtained using bromide-precursors 1,3-dibromo-5,5-dimethyl hydantoin (DBHT),[47] *N*-bromosuccinimide (NBS)[48] and *N*-bromoacetamide (NBA), respectively. The use of the *N*-bromoacetamide (NBA) precursor for the synthesis of NBA-$CsPbBr_3$ NC is indeed a relatively novel approach.

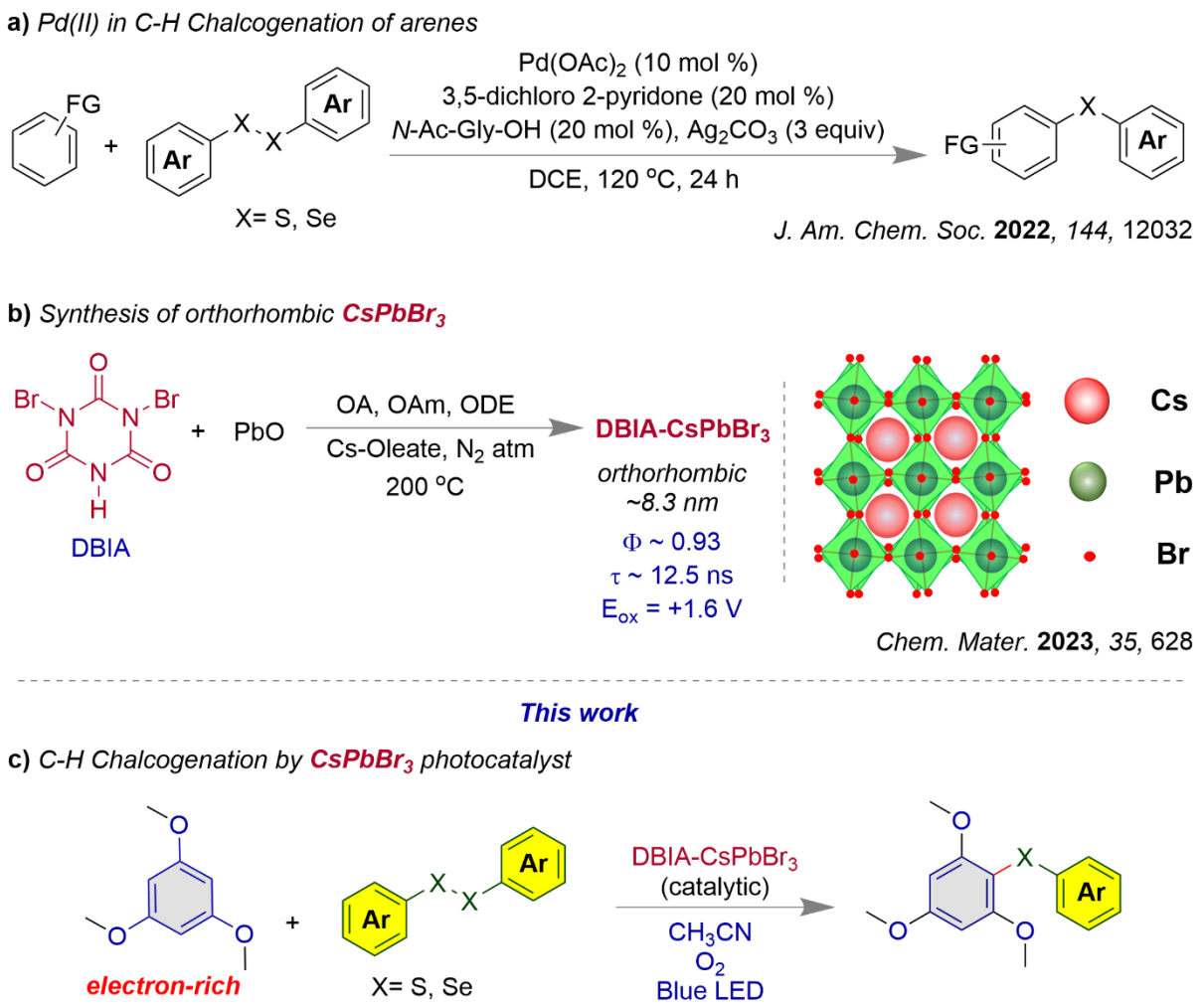

Figure 1. The C-H chalcogenation reactions. a) Pd(II) catalyzed Maiti's report.[41] b) The synthesis of orthorhombic DBIA-$CsPbBr_3$.[45] c) The DBIA-$CsPbBr_3$ as visible light photocatalyst for C-H chalcogenation.

The PXRD pattern showed that the structure of the newly synthesized NBA-$CsPbBr_3$ is also cubic, similar to the DBHT-$CsPbBr_3$[47] and NBS-$CsPbBr_3$,[48] whereas DBIA-$CsPbBr_3$ is orthorhombic (Figure 2a). The images from transmission electron microscopy (TEM) demonstrate the morphologies of the $CsPbBr_3$ NCs and average edge length (8 ~ 8.4 nm) (supporting information). However, the TEM image of the newly synthesized NBA-$CsPbBr_3$ is shown in Figure 2b. In the photophysical study, the colloidal suspension of NCs in hexane exhibited significant broad absorption bands in the visible region (up to 525 nm) (Figure 2c).

All the $CsPbBr_3$ NCs suspension displayed intense green photoluminescence with a comparable quantum yield near unity (Φ ~ 0.92 to 0.99) (Figure 2c).[45, 47-48]

The other factors that can influence the colloidal stability of $CsPbBr_3$ perovskite NCs, are the presence of various aromatic molecules, which can prevent particle aggregation and improve the long-term stability of the NCs.[49-50] We have also established that the electron-rich arenes like methoxy benzenes also been shown to increase the stability of the $CsPbBr_3$ perovskite (supporting information). The fluorescence quenching experiments that were performed with 1,3,5-trimethoxy benzene **1a** (*vide infra*) in acetonitrile under aerobic conditions can provide information about the relative stability of the $CsPbBr_3$ NCs in the presence of electron-rich arenes (Figure 2d). The experiments involved adding **1a** to a solution of $CsPbBr_3$ NCs in acetonitrile and measuring the fluorescence intensity of the solution after 24 h, which remained unchanged with DBIA-$CsPbBr_3$. Contrastingly, NBS-$CsPbBr_3$, DBHT-$CsPbBr_3$ and NBA-$CsPbBr_3$ NCs showed quenching of the fluorescence intensity in acetonitrile in the presence of **1a** (Figure 2d). It is indeed interesting that under aerobic conditions and in polar solvent acetonitrile, the $CsPbBr_3$ NCs showed degradation, and among them, DBIA-$CsPbBr_3$ exhibited better stability in the absence of electron rich arenes.

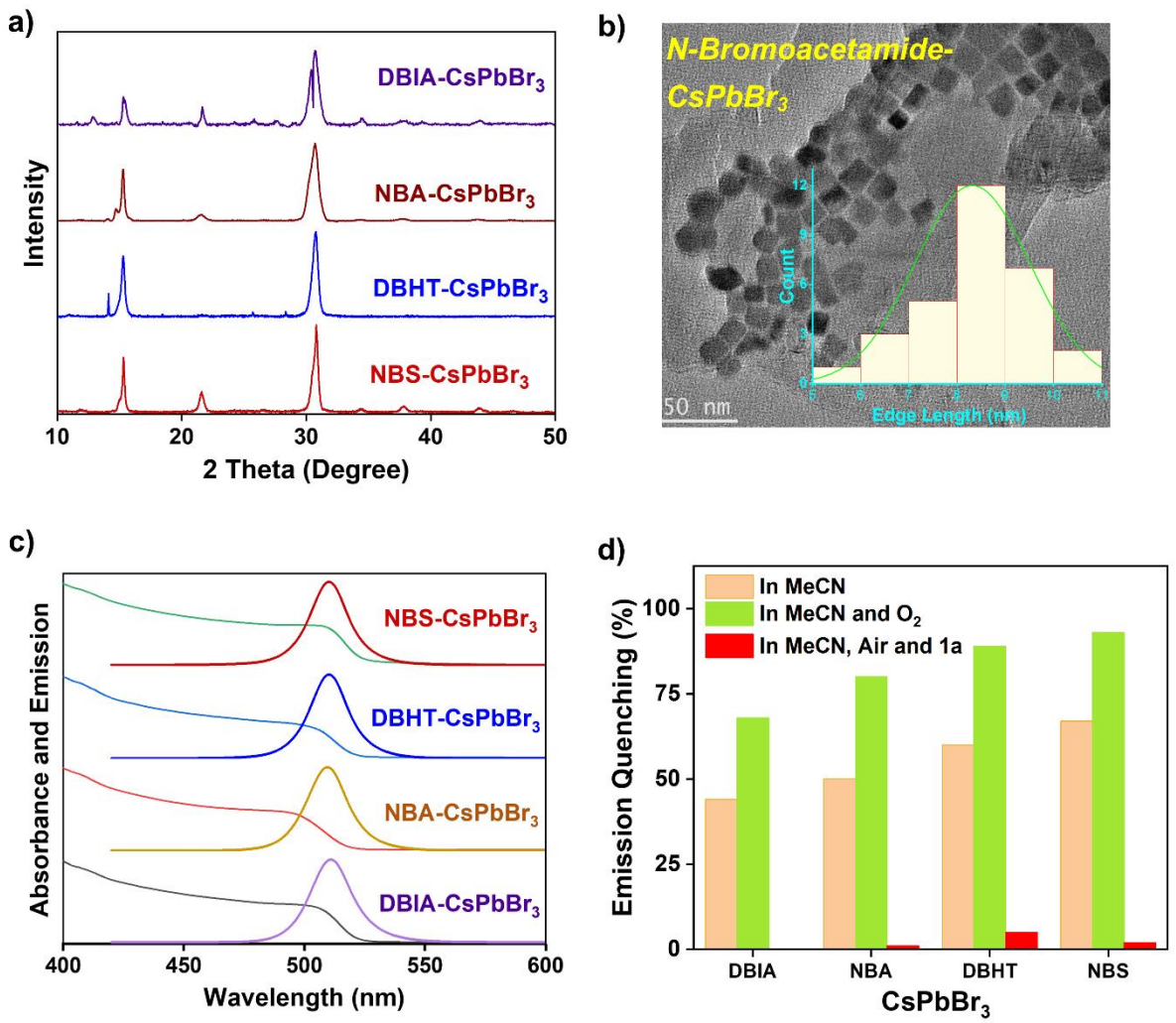

Figure 2. a) PXRD of all the $CsPbBr_3$ NCs. b) TEM image of NBA-$CsPbBr_3$. c) Absorption and emission spectra of all the $CsPbBr_3$ NCs. d) Relative stability of the $CsPbBr_3$ NCs in the presence of electron-rich arene 1,3,5-trimethoixy benzene (**1a**).

The information of optimized reaction conditions provided in Figure 3a and the detail of optimization is given in the supporting information. The synthesis of phenyl(2,4,6-trimethoxyphenyl)sulfane **3aa** was achieved from electron-rich 1,3,5-trimethoxybenzene **1a** (0.35 mmol) and 1,2-diphenyldisulfane **2a** (0.43 mmol) using DBIA-$CsPbBr_3$ (5 mol %) in dry acetonitrile (dielectric constant $\varepsilon \sim 37.5$) and O_2 (aerobic) atmosphere under blue LED ($\lambda \sim 450$ - 455 nm). The results presented in Figure 3b indicate that the yield of compound **3aa** using the DBIA-$CsPbBr_3$ photocatalyst was found to be the highest among the photocatalysts tested,

with a yield of approximately 88%. This is higher compared to the yields obtained using NBS-$CsPbBr_3$ (57%), DBHT-$CsPbBr_3$ (51%), and NBA-$CsPbBr_3$ (75%) photocatalysts. These results suggest that the DBIA-CsPbBr3 photocatalyst is more effective in promoting the reaction to produce **3aa** than the other photocatalysts.

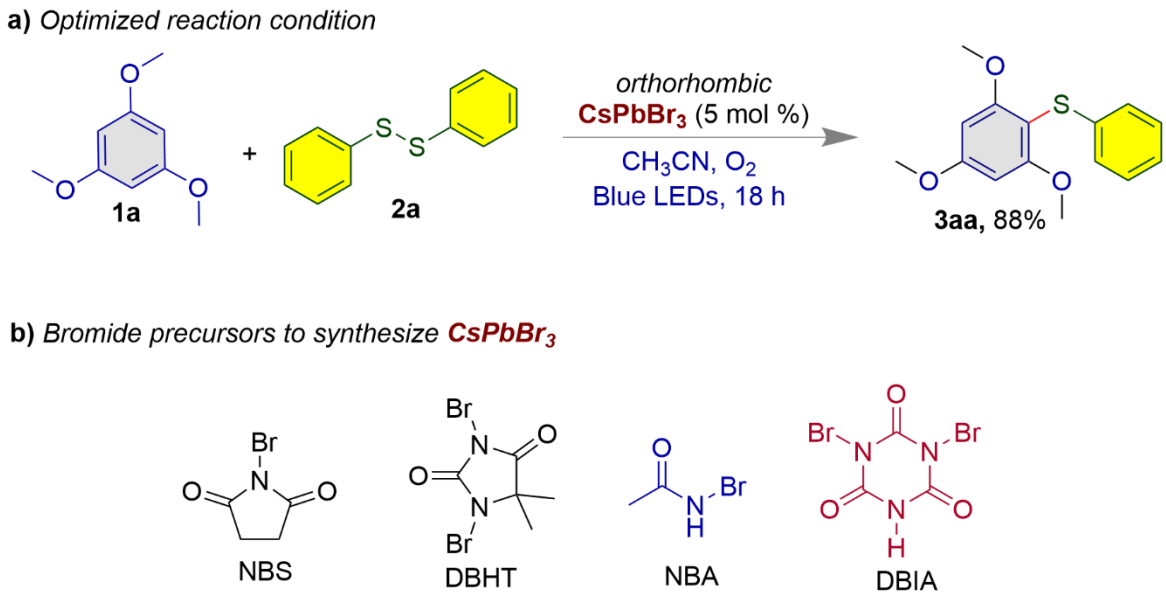

Br – source	Crystal Pattern	Edge Length (nm)	τ (ns)	Φ_{fl}	Yield of 3aa (%)
NBS	Cubic[48]	8.4	9.7	99	57
DBHT	Cubic[47]	8	7.4	92	51
NBA	Cubic (**new**)	8.4	10.2	92	75
DBIA	Orthorhombic[45]	8.3	12.5	93	88

Figure 3. a) The optimized reaction condition. b) Bromide-precursors used for the synthesis of $CsPbBr_3$ NCs and the properties of the NCs.

The photoluminescence lifetime studies were also conducted for the $CsPbBr_3$ NCs ($\tau \sim 7$ to 12.5 ns) (Figure 3b).[45, 47-48, 51] Redox potentials of the $CsPbBr_3$ NCs are determined through cyclic voltammetry (CV) experiments (oxidation potentials, $E_{ox} = +1.6$ V and the reduction potentials, $E_{red} = -1.15 \sim -1.25$V) (Figure S8, supporting information).

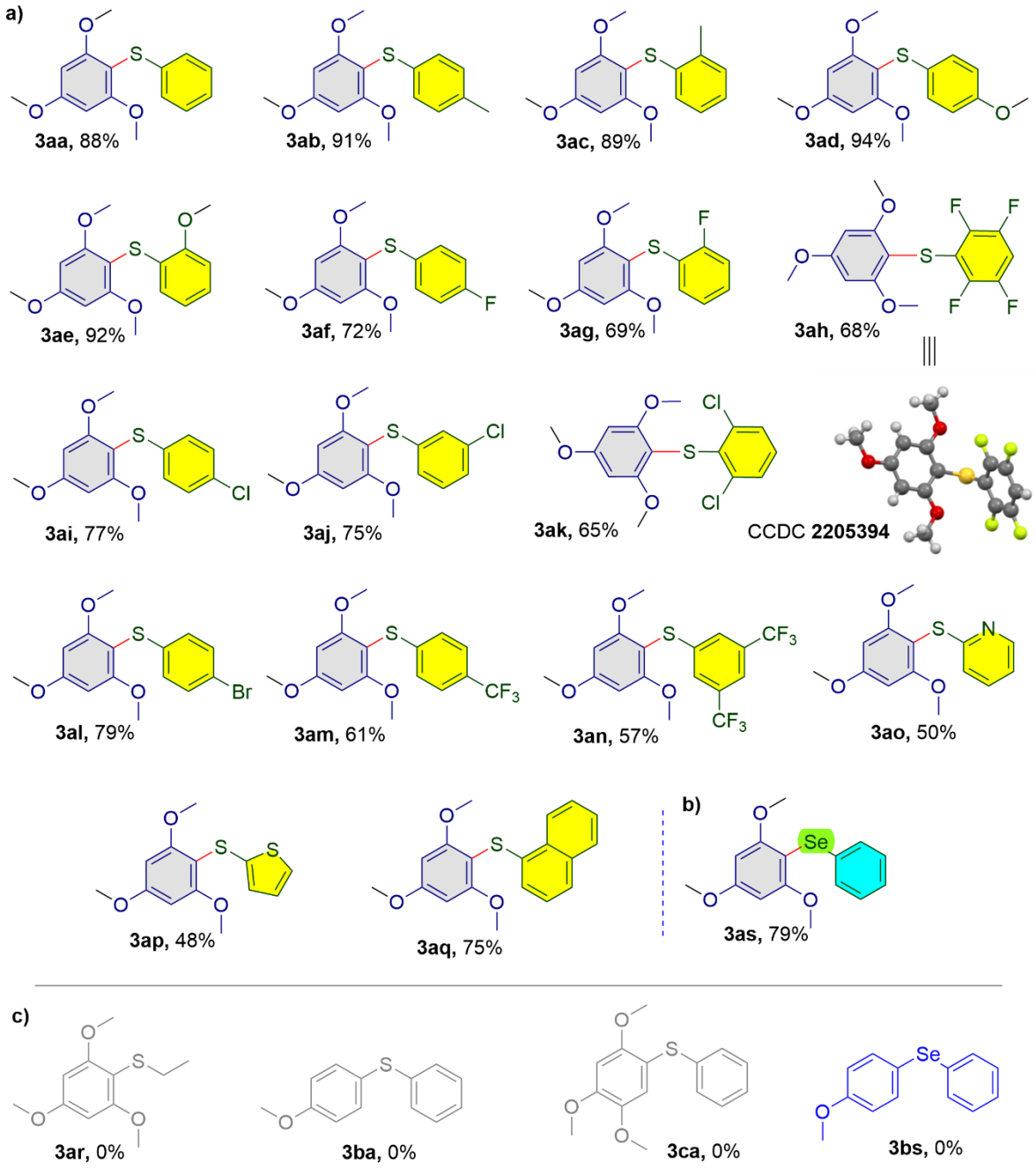

Figure 4. The products from the reactions with a) various disulfides b) and a diselenide. c) Unsuccessful attempts.

The reaction efficiency of different disulfides in the presence of electron-rich arenes is shown in Figure 4a. A variety of disulfides and diselenides were subjected to the reaction under standard conditions. The -Me, and -OMe groups at the *para*- and *ortho*-positions of disulfide produced the corresponding phenyl sulfanes **3aa-3ae** with high yields (88% to 94%). Again, -F containing diaryl disulfides produced thioethers **3af**, **3ag**, and **3ah** with 72%, 69%, and 68% yield, respectively. Next, thioethers **3ai-3ak** having –Cl substituent were synthesized with 65-75% yields. 4-Dibromodiaryl disulfide resulted in **3al** with 79% yield. Compounds **3am** and **3an** were synthesized with 61% and 57% yields, respectively. Furthermore, 1,2-di(thiophen-2-yl)disulfane and 1,2-di(pyridin-2-yl)disulfane reacted well to produce the corresponding thioethers **3ao** and **3ap** with 50% and 48% yields, respectively. Polyaromatic containing disulfide yielded the corresponding diaryl sulfide **3aq** with 75% yield. The coupling reaction between aliphatic disulfide and trimethoxybenzene to produce compound **3ar** failed. The sluggish reaction was observed with anisole under the standard condition. On the other hand, the successful coupling of diaryl diselenide (Figure 4b) with 1,3,5-trimethoxybenzene **1a** to produce **3as** in 79% yield indicates that the reaction conditions were also favorable for this system. The structure of the substrates shown in Figure 4c, which could not be isolated.

The control experiments shown in Figure 5 provided important information about the reaction mechanism. The energy potential diagram shown in Figure 5a, obtained from CV (cyclic voltammetry) experiments, for the photocatalyst (PC) and the reactants **1a** and **2a**. The observation of a lowering of photoluminescence intensity with increasing addition of disulfide suggests that the disulfide quenches the photoluminescence of $CsPbBr_3$ in acetonitrile with a quenching constant of $k_q = 7.52 \times 10^{12}\ s^{-1}\ M^{-1}$ (Figure 5b). The results presented in Figure 5c demonstrate the visual change before and after the reaction under visible light and UV light. The fact that the $CsPbBr_3$ remains crystalline even after the reaction, as shown in Figure S10

(supporting information), suggests that the material retains its structural integrity and is likely to remain catalytically active. The observation of a strong signal in EPR in the trapping experiment in the presence of 5,5-dimethyl-1-pyrroline-*N*-oxide (DMPO, Figure 5d) provides evidence for a radical-based pathway in the reaction.[52] The radical-based mechanism was further supported by the experiments using 1,1-diphenylethylene, 2,2,6,6-tetramethylpiperidine 1-oxyl radical (TEMPO), and butylated hydroxytoluene (BHT) as radical scavengers (Figure 5e). In the light On-OFF-ON experiment (Figure 5f), the reaction was done under three different conditions: once with the light turned on (ON), once with the light turned off (OFF), and once with the light turned on again (ON). By comparing the results of the three conditions, it was established that visible light is indeed essential for the reaction.

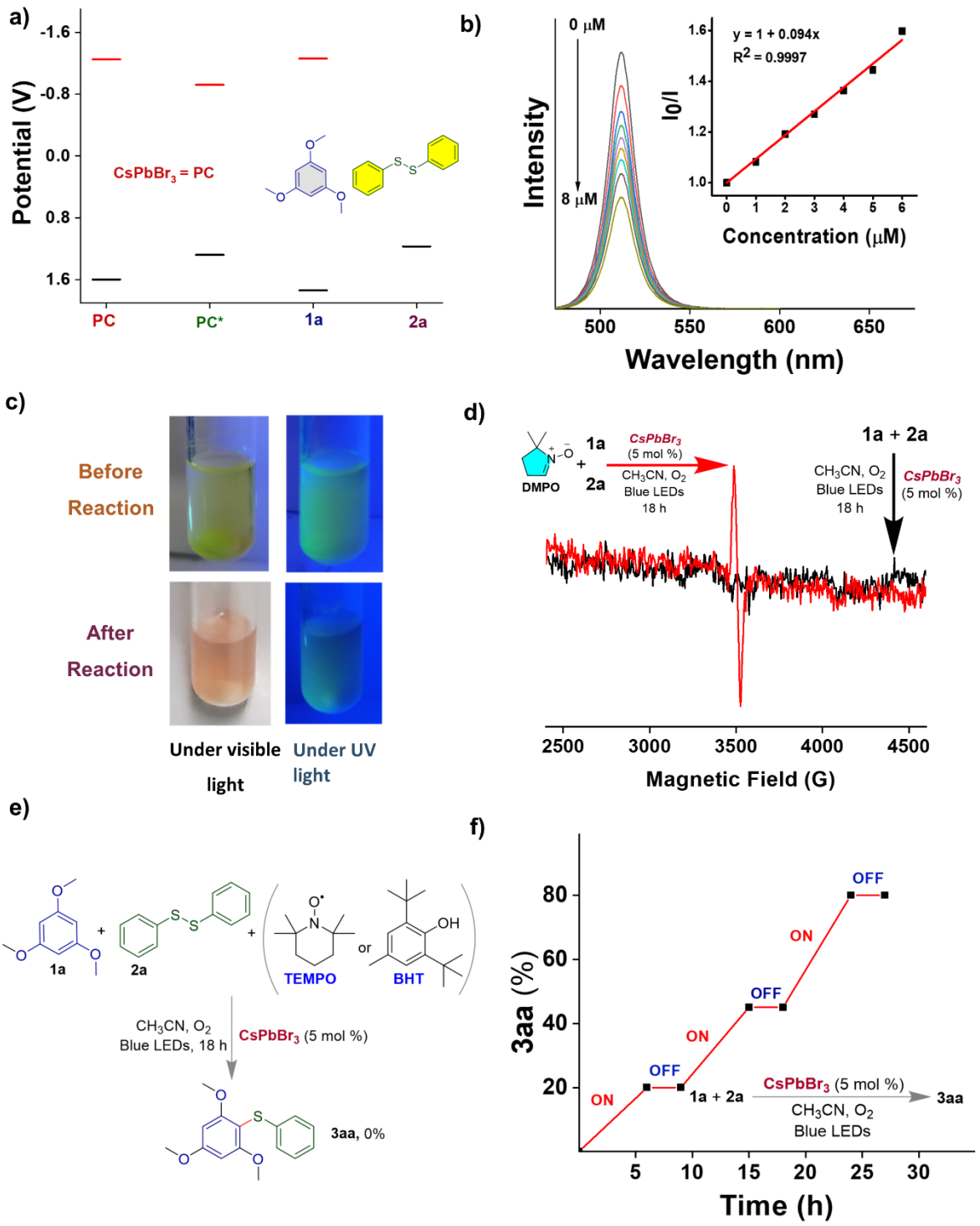

Figure 5. a) Energy potential diagram of the reactants (**1a** and **2a**) and photocatalyst (PC). b) Fluorescence quenching experiment of DBIA-$CsPbBr_3$ upon addition of **2a** in acetonitrile and Stern-Volmer quenching plot (inset). c) Photograph of the reaction mixture before and after irradiation. d) EPR study in the presence of DMPO. e) Radical trapping experiments with TEMPO and BHT. f) The light ON-OFF-ON experiment.

A plausible reaction mechanism is shown in Figure 6a. The presence of a strong absorption band in the visible region of the DBIA-$CsPbBr_3$ NCs makes them susceptible to photochemical excitation after absorption of visible light (blue LED). The disulfide radical cation can be generated through the hole transfer (HT) process from the valence band (VB) of the $CsPbBr_3$ perovskite to the disulfide moiety. The comparison of the redox potentials can provide insights into the driving force for the hole transfer process and the photocatalytic activity of the DBIA-$CsPbBr_3$ NCs (E_{ox} = +1.17 V of disulfide < E^*_{red} = +1.28 V of $CsPbBr_3$) (Figure 5a). The disulfide radical cation generated can react with electron-rich arenes to form intermediate **I**, a radical cation. The superoxide radical anion can be generated through an electron transfer process[53] from the conduction band of the perovskite to molecular oxygen. In this process, the electrons in the conduction band of the perovskite are transferred to molecular oxygen (O_2), forming superoxide radical anions ($O_2^{-\cdot}$). These superoxide radical anions can then react with intermediate **I**, leading to deprotonation and led to the formation of product **3aa** and by-product hydrogen peroxide (H_2O_2). The formation of hydrogen peroxide (H_2O_2) was confirmed by UV-vis spectroscopy through the detection of tri-iodide (I_3^-) in the reaction medium. The detection of tri-iodide is typically performed by adding potassium iodide (KI) and dilute acid to the reaction mixture, which can then be monitored by UV-vis spectroscopy. The appearance of a peak in the UV-vis spectrum at a wavelength of 359 nm was indicative of the formation of tri-iodide, which confirms the presence of hydrogen peroxide in the reaction medium.[54]

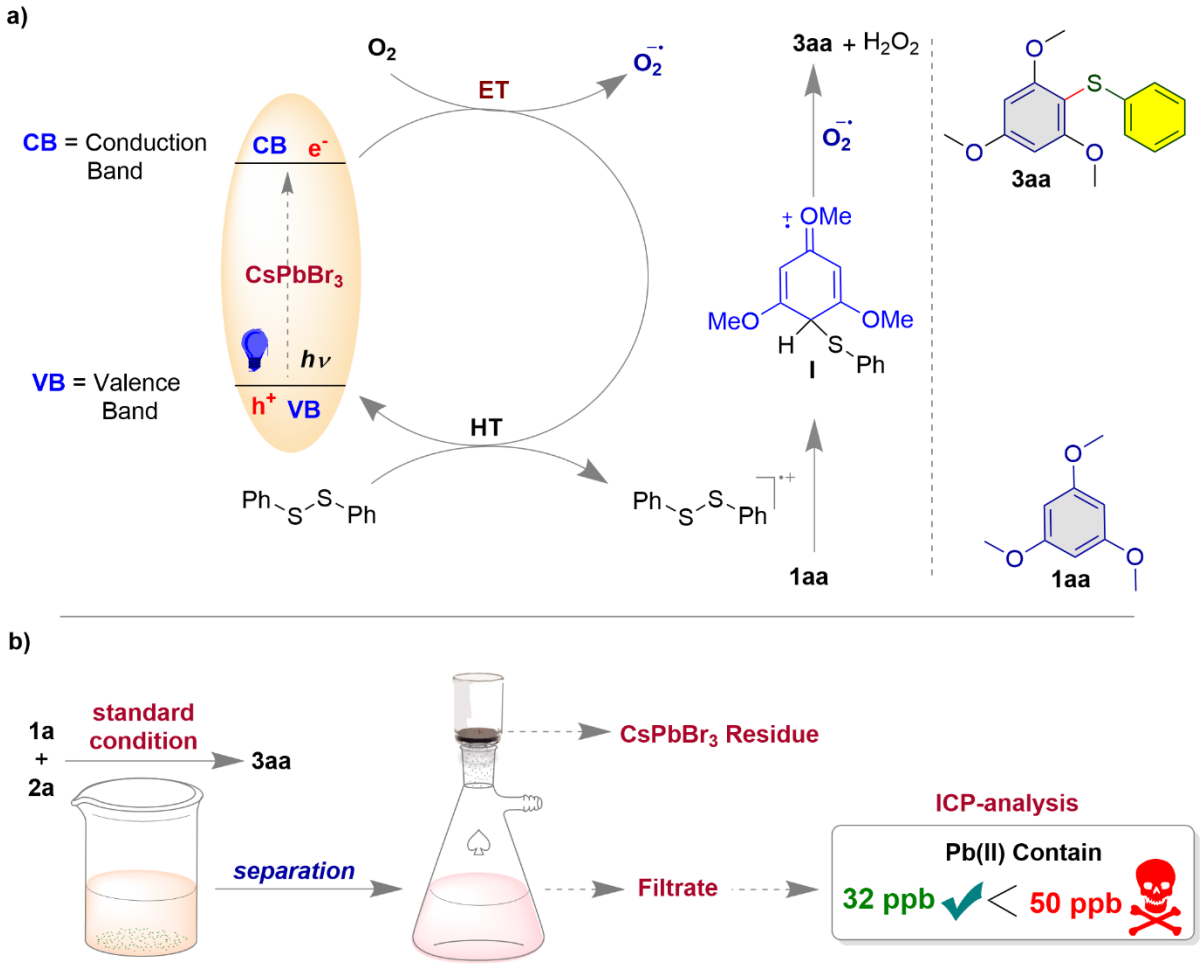

Figure 6. a) Plausible reaction mechanism. b) The lead leaching experiment after the reaction.

The Turn Over Number (TON) measures the catalytic efficiency of the catalyst and in this case, the TON of DBIA-$CsPbBr_3$ NC is 18.11.[55] The perovskite NCs were recovered from the reaction mixture through simple centrifugation (Figure 6b) and the low level of Pb leaching, as indicated by the ICP-OES (inductively coupled plasma optical emission spectrometry) analysis of the filtrate, is also encouraging compare to the previous report.[17] The fact that only 32 ppb (parts per billion) of Pb was leached, shows that this photocatalyst is relatively safe and can be used without significant environmental concern. The maximum allowable amount of lead in drinking water is set at 50 ppb (parts per billion).[56] So, it is possible that DBIA-$CsPbBr_3$ NCs are considered to be environmentally benign visible light photocatalysts.

This is likely due to the unique crystal structure of orthorhombic DBIA-$CsPbBr_3$ perovskite nanocrystals (NCs), which allows for a more efficient transfer of electrons and holes compared to other cubic $CsPbBr_3$ NCs. This leads to a longer photoluminescence lifetime and quantum yields (Φ) compare to the cubic NCs. Importantly, the specific properties of perovskite NCs can also be influenced by other factors such as the modified synthetic methods,[57-60] surface treatment,[5] post-synthetic modifications,[61] etc. The photoluminescence quenching study was carried out of these perovskites in acetonitrile (ACN) and under O_2 atmosphere where orthorhombic $CsPbBr_3$ displayed more stable behavior compare to the cubic $CsPbBr_3$ perovskites (Figure 2d, and Figures S4 and S5, supporting information). The intrinsic stability of orthorhombic DBIA-$CsPbBr_3$ perovskite can be attributed to the fewer crystal defects[62] and higher bromide ion ratios,[63] as these factors contributed to the stability of the orthorhombic $CsPbBr_3$ perovskite. A perovskite NC with fewer crystal defects is less prone to degradation, while a higher bromide ion ratio can improve the overall stability of the material. In addition, we have shown that the electron rich arenes can improve the stability of the perovskite NCs within the reaction system.

Derivatization of the synthesized compounds (diaryl sulfides) is shown in Figure 7. *meta*-Chloroperoxybenzoic acid (*m*CPBA) was used for the oxidation of diaryl sulfide **3aa** into the corresponding sulfoxide (Figure 7a).[64] The Suzuki (Figure 7b)[65] and Sonogashira (Figure 7c)[66] cross-coupling reactions were performed on the compound **3aj**.

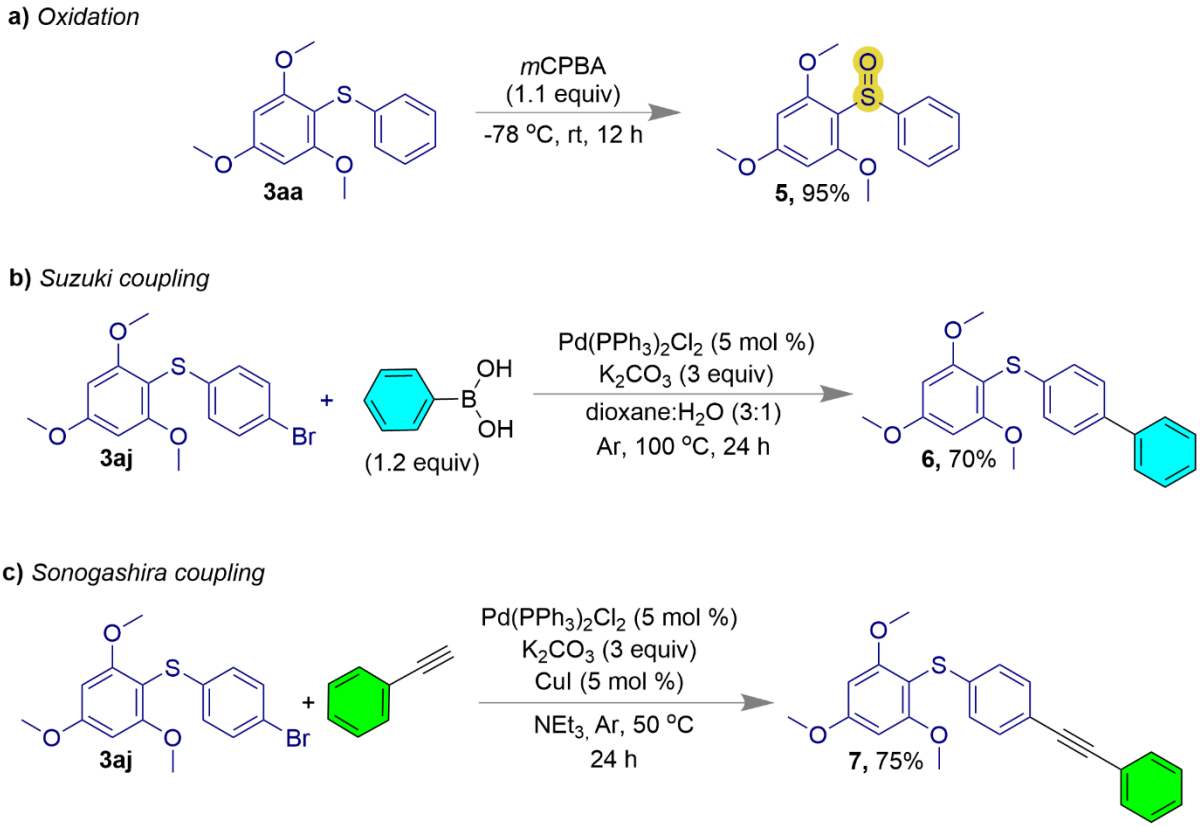

Figure 7. Synthetic utilities of the diaryl sulfides. a) Oxidation of **3aa** using *m*CPBA. b) The Suzuki and c) Sonogashira cross-coupling reactions of **3aj**.

CONCLUSION

In conclusion, the use of an orthorhombic $CsPbBr_3$ perovskite nanocrystal (NC) as visible light photocatalysis, for the synthesis of diaryl sulfides and a diaryl selenide has been reported here. Compared to the cubic-perovskites (NBS-$CsPbBr_3$, DBHT-$CsPbBr_3$ and DBA-$CsPbBr_3$) the orthorhombic DBIA-$CsPbBr_3$ is found to be an efficient visible light photocatalyst under blue LEDs, aerobic condition and in polar solvent like acetonitrile (dielectric constant $\varepsilon \sim 37.5$). The intrinsic stability of the orthorhombic $CsPbBr_3$ was due to the fewer crystal defect and higher bromide ion ratios. In addition, one of the reactants 1,3,5-trimethoxy benzene also helped to increase the stability of the DBIA-$CsPbBr_3$ NC within the reaction system. Due to low lead leaching after the reaction, this NC can also be considered as an environmentally benign

photocatalyst. We anticipate that the results of this work have the potential to provide new insights and guidelines for the fields of synthetic organic and material chemistry.

EXPERIMENTAL SECTION

Chemicals. All the reagents were purchased from commercially available sources and used without further purification. All organic solvents were also received commercially and purified.

Synthesis of DBIA-$CsPbBr_3$ NCs. $CsPbBr_3$ NCs were synthesized according to the literature procedure.[45] Pre-dried Cs_2CO_3 (195 mg, 0.6 mmol), ODE (9 mL), and OA (1.0 mL) were taken in a two-necked 50 mL round-bottom flask (RB). The reaction mixture was dried under vacuum for 30 min at 120 °C and then transferred to the N_2 atmosphere for 1 h, maintaining the same temperature to become a clear solution. In another three-necked 25 mL RB, PbO (44 mg, 0.3 mmol), DBIA (174 mg, 0.6 mmol) and ODE (5 mL, pre-dried) were added respectively. The reaction mixture was kept under vacuum for 30 min at elevated temperature (~120 °C) followed by to the N_2 environment at 130 °C. After 10 min, 1.0 mL OA and 1.0 mL OLA were injected to the reaction mixture and temperature of the reaction mixture was raised to ~200 °C. Then, cesium-oleate (~0.8 mL) solution (preheated at 100 °C) was swiftly injected into the reaction mixture. Subsequently, the reaction was quenched in an ice bath. After that, 3 mL of MeOAc was added to the mixture and centrifuged for 10 min at 6500 rpm. The supernatant was discarded, and the precipitation was dispersed in hexane and kept in the refrigerator for 30 min. The suspension was again centrifuged for 10 min at 6500 rpm. Finally, the supernatant containing the NCs and precipitation were separated and both were stored for future experiments.

Synthesis of NBA-$CsPbBr_3$ NCs. NBA-$CsPbBr_3$ NCs was synthesized using the same procedure as previous using NBA (83 mg, 0.6 mmol).[45]

Synthesis of DBHT-$CsPbBr_3$ NCs. NBA-$CsPbBr_3$ NCs was synthesized following the literature procedure using DBHT (172 mg, 0.6 mmol).[47]

Synthesis of NBS-$CsPbBr_3$ NCs. NBA-$CsPbBr_3$ NCs was synthesized following the literature procedure using NBS (107 mg, 0.6 mmol).[48]

Powder X-ray Diffraction Measurement (PXRD). PXRD pattern was collected using Bruker Davinci D8 diffractometer (Cu-Ka radiation; λ=0.15418 nm). A thin film of the sample was prepared by drop-casting the concentrated suspension of NCs onto a thin quartz plate.

Transmission Electron Microscopy (TEM). TEM images were captured by JEOL (JEM-2100) operating at an accelerating voltage of 200 kV. The sample was prepared on a carbon-coated copper grid by drop-casting the dilute suspension of NCs in hexane.

Energy Dispersive X-ray Spectroscopy (EDX). Energy dispersive X-ray spectra were recorded by Oxford instruments X-MaxN SDD (50 mm2) system and INCA analysis software attached with Carl Zeiss FESEM instrument.

Absorption and Photoluminescence Measurements. UV-VIS absorption and steady-state photoluminescence (PL) spectrum of a colloidal suspension of NCs were recorded with JascoV-730 spectrophotometer and Edinburgh spectrofluorometer FS5 with SC-25 cuvette holder, respectively.

Absolute quantum yield was measured by using an integrating sphere (SC-30).

Time-Correlated Single-Photon Counting. PL decay measurement was carried out through TCSPC method using Edinburgh Instruments (Model OB-920), decorated with 405 nm laser as the excitation source. IRF was determined using a scatter ludox solution. The lifetime profile was fitted with exponential decay function according to the equation, $I(t) = \sum_{i=1}^{n} \alpha_i \exp(-\frac{\tau_i}{t})$ and the average fluorescence lifetime was determined using equation $\tau_{av} = \frac{\sum \alpha_i \tau_i^2}{\sum \alpha_i \tau_i}$; where α_i and τ_i are amplitude and lifetime of ith component respectively.

Photoluminescence Quenching Study. Photoluminescence quenching study of $CsPbBr_3$ was conducted using disulfide as quencher. Through Stern-Volmer kinetics, rate of quenching (k_q) was determined using the equation $I_0/I = 1 + k_q\tau\,[quencher]$, where I_0 is the initial PL intensity without the quencher, I is the intensity after addition of the quencher, and τ is the lifetime of the $CsPbBr_3$. Probe sample was prepared by suspending $CsPbBr_3$ NCs in DCE of concentration 0.5 mg mL^{-1}. Then 20 μL of the concentrate solution was diluted to make a total volume 2 mL. Quencher of concentration of 1 mM was added to the probe suspension in an incremental way of 2 μL maintaining the total volume of 2 mL. Lifetime of $CsPbBr_3$ is ~ 12.5 ns.

Nuclear Magnetic Resonance (NMR) Measurements. NMR spectra were recorded on 400 MHz and 700 MHz (BRUKER® ULTRASHIELD) instruments at 25 °C. The chemical shift values are reported in parts per million (ppm) for residual chloroform (7.26 ppm for ^{1}H and 77.16 ppm for ^{13}C). The peak patterns are designated as follows: s: singlet; d: doublet; t: triplet; q: quartet; m: multiplet; dd: doublet of doublets; td: triplet of doublets; brs: broad singlet. The

coupling constants (*J*) are reported in hertz (Hz). Samples solutions were prepared by dissolving in $CDCl_3$.

High-resolution Mass Spectra (HR-MS). HR-MS were recorded on a TOF Q-II (Bruker) (time of flight) mass spectrometer. Clear solutions of samples were prepared after dissolving in methanol or acetonitrile.

Fourier Transform Infrared Spectroscopy (FTIR). FTIR analysis data were collected from Thermo Scientific (NICOLET iS5) instrument under transmittance mode and reported in wavenumber (cm^{-1}). A thin layer of the compounds on the surface of the KBr pallet was prepared using dichloromethane as a solvent to record the data.

Electron Paramagnetic Resonance (EPR). EPR spectrum was recorded with a Bruker System EMX-microX at 298K and 9.4335 GHz. Typical EPR spectrometer parameters are shown as follows, scan range: 100 G; centre field set: 3480.00 G; time constant: 0.16 ms; scan time: 128.22 s; modulation amplitude: 20.0 G; modulation frequency: 100 kHz; receiver gain: 2.00×10^2; microwave power: $7.14e^{-001}$ mW; g = 2.007092. A description of sample preparation is given later.

Cyclic Voltammetry (CV). Cyclic voltametric data were investigated on the CorrTest Electrochemical Station (Model: CS310, S/N: 1711458) in dry and oxygen-free DCM: hexane (1:4) solution containing 0.1 M tetrabutylammonium hexafluorophosphate as a supporting electrolyte with a decoration of a glassy carbon electrode, a Ag/AgCl electrode and a platinum wire as the working electrode, reference electrode, and counter electrode, respectively using a

scan rate 100 mV/s. Redox potential was referenced against ferrocene/ferrocenium (Fc/Fc^+).

Melting Points. Melting points (mp) of the compounds were determined using a digital melting point apparatus and are uncorrected.

Photoreactor. This photoreactor used obtained from commercial source (Model No.-LED Photochemical reactor CN302, CRYOANO VL- PHOTON). Quartz tubes (LUZCHEM) The intensity of the blue LED is (417 x 100) lx (measured by Sigma-Digital Lux Meter 101, Model: 20036176). Distance between quartz tube and light source was approximately 4.2 cm.

General procedure for the synthesis of 3aa. In an oven dried quartz tube 1,3,5-trimethoxybenzene (0.35 mmol), chalcogens (0.43 mmol), and $CsPbBr_3$ (5 mol %) were dissolved in 2.0 mL dry acetonitrile. After that, the reaction mixture was irradiated by visible light (450-455 nm) for 18 h in the presence of an oxygen balloon. After completion of the reaction, unreacted NCs (photocatalysts) were filtered off, and supernatant acetonitrile was removed under reduced pressure. Then, the crude mixture was diluted in dichloromethane (CH_2Cl_2) and washed with brine solution. The resulting organic solution was dried over anhydrous sodium sulfate and concentrated to obtain a crude mixture which was further purified by silica−gel column chromatography using ethyl acetate and hexane as the eluent to afford the pure product.

The calculation of Turn Over Number (TON). Turn Over Number is calculated by the equation, TON = total mol of product/total mol of catalyst

Molecular weight of $CsPbBr_3$ catalysis is calculated as 579.8 g mol^{-1}

Pb(II) leaching experiment. Pb(II) concentration was estimated using ICP-OES spectrometer (Themo SCIENTIFIC, iCAP 7000 SERIES with autosampler TELEDYNE CETAC TECHNOLOGIES, ASX-280). First 10 mg (5 mol %) $CsPbBr_3$ was dissolved in Millipore water (10% HNO_3) and Pb(II) concentration was determined. Again, after the reaction the solid was separated and the organic solvent was removed from the filtrate followed by the residue was dissolved in Millipore water (10% HNO_3). Then initial and final concentration of Pb(II) was estimated and leaching was calculated.

ASSOCIATED CONTENT

Supporting Information. The file contains: General Information, Synthesis, Crystallographic Data, Compound characterization data, NMR spectra.

AUTHOR INFORMATION

Ashis Mathuri − School of Chemical Sciences, National Institute of Science Education and Research (NISER), Bhubaneswar, Odisha 752050, India.

Buddhadeb Pal− School of Chemical Sciences, National Institute of Science Education and Research (NISER), Bhubaneswar, Odisha 752050, India.

Milan Pramanik – School of Chemical Sciences, National Institute of Science Education and Research (NISER), Bhubaneswar, Odisha 752050, India.

Corresponding Authors

Prasenjit Mal − School of Chemical Sciences, National Institute of Science Education and Research (NISER), Bhubaneswar, Odisha 752050, India. Email pmal@niser.ac.in; ORCID: 0000-0002-7830-9812

Anupam Manna – School of Chemical Sciences, National Institute of Science Education and Research (NISER), Bhubaneswar, Odisha 752050, India. Email anupammanna@niser.ac.in

ACKNOWLEDGMENT

A.M. thank CSIR and B.P. and A.M. thank NISER for fellowship.

REFERENCES

(1) Fu, Y.; Zhu, H.; Chen, J.; Hautzinger, M. P.; Zhu, X. Y.; Jin, S. Metal Halide Perovskite Nanostructures for Optoelectronic Applications and the Study of Physical Properties. *Nat. Rev. Mater.* **2019**, *4*, 169-188.

(2) Al-Ashouri, A.; Köhnen, E.; Li, B.; Magomedov, A.; Hempel, H.; Caprioglio, P.; Márquez, J. A.; Morales Vilches, A. B.; Kasparavicius, E.; Smith, J. A.; Phung, N.; Menzel, D.; Grischek, M.; Kegelmann, L.; Skroblin, D.; Gollwitzer, C.; Malinauskas, T.; Jošt, M.; Matič, G.; Rech, B.; Schlatmann, R.; Topič, M.; Korte, L.; Abate, A.; Stannowski, B.; Neher, D.; Stolterfoht, M.; Unold, T.; Getautis, V.; Albrecht, S. Monolithic Perovskite/Silicon Tandem Solar Cell with >29% Efficiency by Enhanced Hole Extraction. *Science* **2020**, *370*, 1300-1309.

(3) Lu, H.; Liu, Y.; Ahlawat, P.; Mishra, A.; Tress, W. R.; Eickemeyer, F. T.; Yang, Y.; Fu, F.; Wang, Z.; Avalos, C. E.; Carlsen, B. I.; Agarwalla, A.; Zhang, X.; Li, X.; Zhan, Y.; Zakeeruddin, S. M.; Emsley, L.; Rothlisberger, U.; Zheng, L.; Hagfeldt, A.; Grätzel, M. Vapor-Assisted Deposition of Highly Efficient, Stable Black-Phase $FAPbI_3$ Perovskite Solar Cells. *Science* **2020**, *370*, eabb8985.

(4) Jeong, J.; Kim, M.; Seo, J.; Lu, H.; Ahlawat, P.; Mishra, A.; Yang, Y.; Hope, M. A.; Eickemeyer, F. T.; Kim, M.; Yoon, Y. J.; Choi, I. W.; Darwich, B. P.; Choi, S. J.; Jo, Y.; Lee, J. H.; Walker, B.; Zakeeruddin, S. M.; Emsley, L.; Rothlisberger, U.; Hagfeldt, A.; Kim, D. S.; Grätzel, M.; Kim, J. Y. Pseudo-Halide Anion Engineering for α-$FAPbI_3$ Perovskite Solar Cells. *Nature* **2021**, *592*, 381-385.

(5) Garai, R.; Gupta, R. K.; Hossain, M.; Iyer, P. K. Surface Recrystallized Stable 2d–3d Graded Perovskite Solar Cells for Efficiency Beyond 21%. *J. Mater. Chem. A* **2021**, *9*, 26069-26076.

(6) Kim, H.; Zhao, L.; Price, J. S.; Grede, A. J.; Roh, K.; Brigeman, A. N.; Lopez, M.; Rand, B. P.; Giebink, N. C. Hybrid Perovskite Light Emitting Diodes under Intense Electrical Excitation. *Nat. Commun.* **2018**, *9*, 4893.

(7) Cho, H.; Jeong, S.-H.; Park, M.-H.; Kim, Y.-H.; Wolf, C.; Lee, C.-L.; Heo, J. H.; Sadhanala, A.; Myoung, N.; Yoo, S.; Im, S. H.; Friend, R. H.; Lee, T.-W. Overcoming the Electroluminescence Efficiency Limitations of Perovskite Light-Emitting Diodes. *Science* **2015**, *350*, 1222-1225.

(8) Zhang, Q.; Shang, Q.; Su, R.; Do, T. T. H.; Xiong, Q. Halide Perovskite Semiconductor Lasers: Materials, Cavity Design, and Low Threshold. *Nano Lett.* **2021**, *21*, 1903-1914.

(9) Zhizhchenko, A.; Syubaev, S.; Berestennikov, A.; Yulin, A. V.; Porfirev, A.; Pushkarev, A.; Shishkin, I.; Golokhvast, K.; Bogdanov, A. A.; Zakhidov, A. A.; Kuchmizhak, A. A.; Kivshar, Y. S.; Makarov, S. V. Single-Mode Lasing from Imprinted Halide-Perovskite Microdisks. *ACS Nano* **2019**, *13*, 4140-4147.

(10) Deng, W.; Huang, L.; Xu, X.; Zhang, X.; Jin, X.; Lee, S.-T.; Jie, J. Ultrahigh-Responsivity Photodetectors from Perovskite Nanowire Arrays for Sequentially Tunable Spectral Measurement. *Nano Lett.* **2017**, *17*, 2482-2489.

(11) Kumar, A.; Kumar, A.; Krishnan, V. Perovskite Oxide Based Materials for Energy and Environment-Oriented Photocatalysis. *ACS Catal.* **2020**, *10*, 10253-10315.

(12) Sun, Q.-M.; Xu, J.-J.; Tao, F.-F.; Ye, W.; Zhou, C.; He, J.-H.; Lu, J.-M. Boosted Inner Surface Charge Transfer in Perovskite Nanodots@Mesoporous Titania Frameworks for Efficient and Selective Photocatalytic CO_2 Reduction to Methane. *Angew. Chem. Int. Ed.* **2022**, *61*, e202200872.

(13) Huang, H.; Pradhan, B.; Hofkens, J.; Roeffaers, M. B. J.; Steele, J. A. Solar-Driven Metal Halide Perovskite Photocatalysis: Design, Stability, and Performance. *ACS Energy Lett.* **2020**, *5*, 1107-1123.

(14) Cardenas-Morcoso, D.; Gualdrón-Reyes, A. F.; Ferreira Vitoreti, A. B.; García-Tecedor, M.; Yoon, S. J.; Solis de la Fuente, M.; Mora-Seró, I.; Gimenez, S. Photocatalytic and Photoelectrochemical Degradation of Organic Compounds with All-Inorganic Metal Halide Perovskite Quantum Dots. *J. Phys. Chem. Lett.* **2019**, *10*, 630-636.

(15) Quan, L. N.; Rand, B. P.; Friend, R. H.; Mhaisalkar, S. G.; Lee, T.-W.; Sargent, E. H. Perovskites for Next-Generation Optical Sources. *Chem. Rev.* **2019**, *119*, 7444-7477.

(16) Gurung, B.; Pradhan, S.; Sharma, D.; Bhujel, D.; Basel, S.; Chettri, S.; Rasaily, S.; Pariyar, A.; Tamang, S. $CsPbBr_3$ Perovskite Quantum Dots as a Visible Light Photocatalyst for Cyclisation of Diamines and Amino Alcohols: An Efficient Approach to Synthesize Imidazolidines, Fused-Imidazolidines and Oxazolidines. *Catal. Sci. Technol.* **2022**, *12*, 5891-5898.

(17) Shi, A.; Sun, K.; Chen, X.; Qu, L.; Zhao, Y.; Yu, B. Perovskite as Recyclable Photocatalyst for Annulation Reaction of N-Sulfonyl Ketimines. *Org. Lett.* **2022**, *24*, 299-303.

(18) Wu, W.-B.; Wong, Y.-C.; Tan, Z.-K.; Wu, J. Photo-Induced Thiol Coupling and C–H Activation Using Nanocrystalline Lead-Halide Perovskite Catalysts. *Catal. Sci. Technol.* **2018**, *8*, 4257-4263.

(19) Wang, K.; Lu, H.; Zhu, X.; Lin, Y.; Beard, M. C.; Yan, Y.; Chen, X. Ultrafast Reaction Mechanisms in Perovskite Based Photocatalytic C–C Coupling. *ACS Energy Lett.* **2020**, *5*, 566-571.

(20) Zhu, X.; Lin, Y.; Sun, Y.; Beard, M. C.; Yan, Y. Lead-Halide Perovskites for Photocatalytic α-Alkylation of Aldehydes. *J. Am. Chem. Soc.* **2019**, *141*, 733-738.

(21) Li, Y.; Wang, T.; Wang, Y.; Deng, Z.; Zhang, L.; Zhu, A.; Huang, Y.; Zhang, C.; Yuan, M.; Xie, W. Tunable Photocatalytic Two-Electron Shuttle between Paired Redox Sites on Halide Perovskite Nanocrystals. *ACS Catal.* **2022**, *12*, 5903-5910.

(22) Tlili, A.; Lakhdar, S. Acridinium Salts and Cyanoarenes as Powerful Photocatalysts: Opportunities in Organic Synthesis. *Angew. Chem. Int. Ed.* **2021**, *60*, 19526-19549.

(23) Chan, A. Y.; Perry, I. B.; Bissonnette, N. B.; Buksh, B. F.; Edwards, G. A.; Frye, L. I.; Garry, O. L.; Lavagnino, M. N.; Li, B. X.; Liang, Y.; Mao, E.; Millet, A.; Oakley, J. V.; Reed, N. L.; Sakai, H. A.; Seath, C. P.; MacMillan, D. W. C. Metallaphotoredox: The Merger of Photoredox and Transition Metal Catalysis. *Chem. Rev.* **2022**, *122*, 1485-1542.

(24) Steele, J. A.; Braeckevelt, T.; Prakasam, V.; Degutis, G.; Yuan, H.; Jin, H.; Solano, E.; Puech, P.; Basak, S.; Pintor-Monroy, M. I.; Van Gorp, H.; Fleury, G.; Yang, R. X.; Lin, Z.; Huang, H.; Debroye, E.; Chernyshov, D.; Chen, B.; Wei, M.; Hou, Y.; Gehlhaar, R.; Genoe, J.; De Feyter, S.; Rogge, S. M. J.; Walsh, A.; Sargent, E. H.; Yang, P.; Hofkens, J.; Van Speybroeck, V.; Roeffaers, M. B. J. An Embedded Interfacial Network Stabilizes Inorganic $CsPbI_3$ Perovskite Thin Films. *Nat. Commun.* **2022**, *13*, 7513.

(25) Boyd, C. C.; Cheacharoen, R.; Leijtens, T.; McGehee, M. D. Understanding Degradation Mechanisms and Improving Stability of Perovskite Photovoltaics. *Chem. Rev.* **2019**, *119*, 3418-3451.

(26) Mateker, W. R.; McGehee, M. D. Progress in Understanding Degradation Mechanisms and Improving Stability in Organic Photovoltaics. *Adv. Mater.* **2017**, *29*, 1603940.

(27) Zhang, Z.; Tian, X.; Wang, C.; Jin, J.; Jiang, Y.; Zhou, Q.; Zhu, J.; Xu, J.; He, R.; Huang, Y.; Ren, S.; Chen, C.; Gao, P.; Long, R.; Zhao, D. Revealing Superoxide-Induced Degradation in Lead-Free Tin Perovskite Solar Cells. *Energy Environ. Sci.* **2022**, *15*, 5274-5283.

(28) Wang, R.; Mujahid, M.; Duan, Y.; Wang, Z.-K.; Xue, J.; Yang, Y. A Review of Perovskites Solar Cell Stability. *Adv. Funct. Mater.* **2019**, *29*, 1808843.

(29) Otero-Martínez, C.; Fiuza-Maneiro, N.; Polavarapu, L. Enhancing the Intrinsic and Extrinsic Stability of Halide Perovskite Nanocrystals for Efficient and Durable Optoelectronics. *ACS Appl. Mater. Interfaces* **2022**, *14*, 34291-34302.

(30) Slotcavage, D. J.; Karunadasa, H. I.; McGehee, M. D. Light-Induced Phase Segregation in Halide-Perovskite Absorbers. *ACS Energy Lett.* **2016**, *1*, 1199-1205.

(31) Kim, B. J.; Kim, D. H.; Kwon, S. L.; Park, S. Y.; Li, Z.; Zhu, K.; Jung, H. S. Selective Dissolution of Halide Perovskites as a Step Towards Recycling Solar Cells. *Nat. Commun.* **2016**, *7*, 11735.

(32) Akkerman, Q. A.; Rainò, G.; Kovalenko, M. V.; Manna, L. Genesis, Challenges and Opportunities for Colloidal Lead Halide Perovskite Nanocrystals. *Nat. Mater.* **2018**, *17*, 394-405.

(33) Boudreault, P.-L. T.; Najari, A.; Leclerc, M. Processable Low-Bandgap Polymers for Photovoltaic Applications. *Chem. Mater.* **2011**, *23*, 456-469.

(34) Qiu, R.; Reddy, V. P.; Iwasaki, T.; Kambe, N. The Palladium-Catalyzed Intermolecular C-H Chalcogenation of Arenes. *J. Org. Chem.* **2015**, *80*, 367-374.

(35) Zhao, C.; Rakesh, K. P.; Ravidar, L.; Fang, W.-Y.; Qin, H.-L. Pharmaceutical and Medicinal Significance of Sulfur (SVI)-Containing Motifs for Drug Discovery: A Critical Review. *Eur. J. Med. Chem.* **2019**, *162*, 679-734.

(36) Gandeepan, P.; Koeller, J.; Ackermann, L. Expedient C–H Chalcogenation of Indolines and Indoles by Positional-Selective Copper Catalysis. *ACS Catal.* **2017**, *7*, 1030-1034.

(37) Sharma, U. K.; Gemoets, H. P. L.; Schröder, F.; Noël, T.; Van der Eycken, E. V. Merger of Visible-Light Photoredox Catalysis and C–H Activation for the Room-

Temperature C-2 Acylation of Indoles in Batch and Flow. *ACS Catal.* **2017**, *7*, 3818-3823.

(38) Qin, Y.; Zhu, L.; Luo, S. Organocatalysis in Inert C–H Bond Functionalization. *Chem. Rev.* **2017**, *117*, 9433-9520.

(39) Pramanik, M.; Choudhuri, K.; Mal, P. Metal-Free C–S Coupling of Thiols and Disulfides. *Org. Biomol. Chem.* **2020**, *18*, 8771-8792.

(40) Choudhuri, K.; Pramanik, M.; Mal, P. Noncovalent Interactions in C–S Bond Formation Reactions. *J. Org. Chem.* **2020**, *85*, 11997-12011.

(41) Sinha, S. K.; Panja, S.; Grover, J.; Hazra, P. S.; Pandit, S.; Bairagi, Y.; Zhang, X.; Maiti, D. Dual Ligand Enabled Nondirected C–H Chalcogenation of Arenes and Heteroarenes. *J. Am. Chem. Soc.* **2022**, *144*, 12032-12042.

(42) Huang, Z.; Zhang, D.; Qi, X.; Yan, Z.; Wang, M.; Yan, H.; Lei, A. Radical-Radical Cross-Coupling for C-S Bond Formation. *Org. Lett.* **2016**, *18*, 2351-2354.

(43) Protesescu, L.; Yakunin, S.; Bodnarchuk, M. I.; Krieg, F.; Caputo, R.; Hendon, C. H.; Yang, R. X.; Walsh, A.; Kovalenko, M. V. Nanocrystals of Cesium Lead Halide Perovskites ($CsPbX_3$, X = Cl, Br, and I): Novel Optoelectronic Materials Showing Bright Emission with Wide Color Gamut. *Nano Lett.* **2015**, *15*, 3692-3696.

(44) Vighnesh, K.; Wang, S.; Liu, H.; Rogach, A. L. Hot-Injection Synthesis Protocol for Green-Emitting Cesium Lead Bromide Perovskite Nanocrystals. *ACS Nano* **2022**, *16*, 19618-19625.

(45) Manna, A.; Dinda, T. K.; Ghosh, S.; Mal, P. $CsPbBr_3$ in the Activation of the C–Br Bond of $CBrX_3$ (X = Cl, Br) under Sunlight. *Chem. Mater.* **2023**, *35*, 628-637.

(46) Zhang, B.; Altamura, D.; Caliandro, R.; Giannini, C.; Peng, L.; De Trizio, L.; Manna, L. Stable $CsPbBr_3$ Nanoclusters Feature a Disk-Like Shape and a Distorted Orthorhombic Structure. *J. Am. Chem. Soc.* **2022**, *144*, 5059-5066.

(47) Mahankudo, S. K.; Das, A.; Mishra, K.; Barai, M.; Mal, P.; Ghosh, S. Synthesis of Cs/Methylammonium/Formamidinium $PbBr_3$ Perovskite Nanocrystals with Green Emissions: Implications for Display Applications. *ACS Appl. Nano Mater.* **2022**, *5*, 4360-4366.

(48) Paul, S.; Samanta, A. N-Bromosuccinimide as Bromide Precursor for Direct Synthesis of Stable and Highly Luminescent Green-Emitting Perovskite Nanocrystals. *ACS Energy Lett.* **2020**, *5*, 64-69.

(49) Kim, J.; Yun, A. J.; Gil, B.; Lee, Y.; Park, B. Triamine-Based Aromatic Cation as a Novel Stabilizer for Efficient Perovskite Solar Cells. *Adv. Funct. Mater.* **2019**, *29*, 1905190.

(50) Dutt, V. G. V.; Akhil, S.; Mishra, N. Enhancement of Photoluminescence and the Stability of $CsPbX_3$ (X = Cl, Br, and I) Perovskite Nanocrystals with Phthalimide Passivation. *Nanoscale* **2021**, *13*, 14442-14449.

(51) Imran, M.; Caligiuri, V.; Wang, M.; Goldoni, L.; Prato, M.; Krahne, R.; De Trizio, L.; Manna, L. Benzoyl Halides as Alternative Precursors for the Colloidal Synthesis of Lead-Based Halide Perovskite Nanocrystals. *J. Am. Chem. Soc.* **2018**, *140*, 2656-2664.

(52) Wang, H.; Li, Y.; Tang, Z.; Wang, S.; Zhang, H.; Cong, H.; Lei, A. Z-Selective Addition of Diaryl Phosphine Oxides to Alkynes Via Photoredox Catalysis. *ACS Catal.* **2018**, *8*, 10599-10605.

(53) Liang, G.; Wang, J.-H.; Lei, T.; Cheng, Y.-Y.; Zhou, C.; Chen, Y.-J.; Ye, C.; Chen, B.; Tung, C.-H.; Wu, L.-Z. Direct C–H Thiolation for Selective Cross-Coupling of Arenes with Thiophenols Via Aerobic Visible-Light Catalysis. *Org. Lett.* **2021**, *23*, 8082-8087.

(54) Ang, D.; Harmonis; Yuk; Ung; Ei, S. N.; On, A.; Eon; Ong, J. J. C.; Yuseok Determination of Triiodide Ion Concentration Using UV-Visible Spectrophotometry. *Asian J. Chem.* **2014**, *26*, 4084-4086.

(55) Zhu, X.; Lin, Y.; San Martin, J.; Sun, Y.; Zhu, D.; Yan, Y. Lead Halide Perovskites for Photocatalytic Organic Synthesis. *Nat. Commun.* **2019**, *10*, 2843.

(56) Kumar, M.; Puri, A. A Review of Permissible Limits of Drinking Water. *Indian J. Occup. Environ. Med.* **2012**, *16*, 40-44.

(57) Bera, S.; Behera, R. K.; Pradhan, N. α-Halo Ketone for Polyhedral Perovskite Nanocrystals: Evolutions, Shape Conversions, Ligand Chemistry, and Self-Assembly. *J. Am. Chem. Soc.* **2020**, *142*, 20865-20874.

(58) Dutta, A.; Behera, R. K.; Pal, P.; Baitalik, S.; Pradhan, N. Near-Unity Photoluminescence Quantum Efficiency for All $CsPbX_3$ (X=Cl, Br, and I) Perovskite Nanocrystals: A Generic Synthesis Approach. *Angew. Chem. Int. Ed.* **2019**, *58*, 5552-5556.

(59) Pradhan, N. Tips and Twists in Making High Photoluminescence Quantum Yield Perovskite Nanocrystals. *ACS Energy Lett.* **2019**, *4*, 1634-1638.

(60) Stelmakh, A.; Aebli, M.; Baumketner, A.; Kovalenko, M. V. On the Mechanism of Alkylammonium Ligands Binding to the Surface of $CsPbBr_3$ Nanocrystals. *Chem. Mater.* **2021**, *33*, 5962-5973.

(61) Shamsi, J.; Urban, A. S.; Imran, M.; De Trizio, L.; Manna, L. Metal Halide Perovskite Nanocrystals: Synthesis, Post-Synthesis Modifications, and Their Optical Properties. *Chem. Rev.* **2019**, *119*, 3296-3348.

(62) Bera, S.; Saha, A.; Mondal, S.; Biswas, A.; Mallick, S.; Chatterjee, R.; Roy, S. Review of Defect Engineering in Perovskites for Photovoltaic Application. *Mater. Adv.* **2022**, *3*, 5234-5247.

(63) Akhil, S.; Palabathuni, M.; Biswas, S.; Singh, R.; Mishra, N. Highly Stable Amine-Free $CsPbBr_3$ Perovskite Nanocrystals for Perovskite-Based Display Applications. *ACS Appl. Nano Mater.* **2022**, *5*, 13561-13572.

(64) Pramanik, M.; Mathuri, A.; Mal, P. Sulfur⋯Oxygen Interaction-Controlled (Z)-Selective Anti-Markovnikov Vinyl Sulfides. *Chem. Commun.* **2021**, *57*, 5698-5701.

(65) Martin, R.; Buchwald, S. L. Palladium-Catalyzed Suzuki−Miyaura Cross-Coupling Reactions Employing Dialkylbiaryl Phosphine Ligands. *Acc. Chem. Res.* **2008**, *41*, 1461-1473.

(66) Chinchilla, R.; Nájera, C. The Sonogashira Reaction: A Booming Methodology in Synthetic Organic Chemistry. *Chem. Rev.* **2007**, *107*, 874-922.